Supporting Information

Improving the performance of a triboelectric nanogenerator by tuning the work functionof a surface modified tribonegativepolymer composite

Manisha Kundu[a,b], Monisha Sarkar[a], Sumana Lakshman[a], SwarnenduBanerjee[d], Matej Hývl[d], Martin Ledinský[d], Ruma Basu[b], NavonilBose[a,c*], Sukhen Das[a*]

[a]Department of Physics, Jadavpur University, Kolkata-700032, India.
[b]Department of Physics, Jogamaya Devi College, Kolkata-700026, India.
[c]Supreme Knowledge Foundation Group of Institutions, Mankundu, Hooghly-712139 India.
[d]Institute of Physics of the Czech Academy of Sciences, Cukrovarnicka 10, 16200, Prague, Czech Republic.

Corresponding Authors' Email Address:
Navonil Bose: navonil05@gmail.com
Sukhen Das: sdasphysics@gmail.com

S1 Experimental

Materials

99.98% Sodium molybdate dihydrate ($Na_2MoO_4.2H_2O$, Merck, Germany), Polyethylene glycol [$H(OCH_2CH_2)_nOH$] (PEG-6000, Merck, Germany), and 37 % pure hydrochloric acid (HCl) are used for the nanofiller synthesis. For the nanocomposite film synthesis, Poly(vinylidene fluoride-co-hexa-fluoropropylene) (PVDF-HFP) pellets (Mw 4,55,500 g mol^{-1}, Sigma Aldrich, USA) and Dry N,N-dimethylformamide (DMF, Merck, India) are used. All chemicals are analytical grade and used without further purification.

Instrumentation

X-Ray diffractometer D8 Advance, Bruker, is used to obtain the XRD diffraction peaks at 2θ ranging from 10˚ to 50˚ with wavelength $\lambda_{Cu-K\alpha} = 1.5418$ Å. Field Emission Scanning Electron Microscope (FESEM) INSPECT F50 is used to analyze the surface morphology of both surfaces of the nanocomposite films. Fourier-Transform Infrared Spectrophotometer IRAffinity-1S, Shimadzu, is used to study α- and β-phase vibrations and confirm the beta phase enhancement of the different nanocomposites in the wavenumber range of 500-1000 cm^{-1} in the absorbance mode. The energy harvesting performance and the bending angle monitoring studies are carried out using the Digital Storage Oscilloscope, Siglent. The short-circuit current measurement of the device is performed by

using Keithley DAQ6510 multimeter system (1MSample/S). Atomic Force Microscopy (AFM) was employed with the Bruker Dimension ICON to acquire sample topography and contact potential difference (CPD) signals via an amplitude-modulated two-pass technique (AM-KPFM). For all the measurements, a doped-diamond coated DDESP-V2 (Bruker) probe was used with a tip radius of 100-120 nm, tip back and front angles of 17.5 ± 2.5 and 25 ± 2.5°, respectively, and an Sb-Si cantilever with Al backside coating.

Synthesisof MoO_3 nanoflakes

The 2Dα-phase MoO_3 nanoparticles are synthesized through a simple modified co-precipitation method. PEG 6000, used as a surfactant, is completely dissolved in an aqueous solution and mixed with stoichiometric amounts of $Na_2MoO_4.2H_2O$. The solution is allowed to stir continuously to ensure homogeneity and the temperature raised to 100 ˚C. HCl is added dropwise to the mixture in order to maintain a constant pH during the formation of the nanoparticles. The reaction is allowed to continue till the formation of precipitate which is then collected through centrifugation, washed, and dried overnight.

Synthesis of the MoO_3/PVDF-HFP nanocomposite films

2D MoO_3 loaded PVDF-HFP nanocomposite films are fabricated using the phase inversion method. 500 mg PVDF-HFP is completely dissolved in 5ml DMF and calculated weight percentages (0%, 1%, 2%, 3%, and 4%) of the synthesized nanoparticles are added to the solution. A homogenous composition is obtained by allowing the mixture to stir overnight. For casting the nanocomposite films, a well having dimension 4 cm × 4 cm × 80 μm is created on a clean glass plate and 1 ml of the solution is poured in. The solution is uniformly distributed in the well using the doctor's blade method and the glass plate is dipped in a water coagulation bath for 10 minutes. After the formation of the film, the glass plate is removed from the water bath and dried on a hot plate for one hour. The film is allowed to cool and peeled off the glass plate to obtain the various percentage loaded MoO_3/PVDF-HFP nanocomposite films (MPI00, MPI01, MPI02, MPI03, and MPI04, respectively).

S2 Characterization of MoO_3 nanofiller

The structural analysis of the as synthesized nanoparticles is carried out using the x-ray diffraction analysis as displayed in Figure S1 (a). The peaks are well matched with the ICDD card no. 96-900-9670 indicating the successful synthesis of the orthorhombic MoO_3 (α-MoO_3) nanoparticles (space group = Pn m a (62)). Further, the presence of well-formed distinct peaks suggest the formation of pure, single-phase, crystalline α-MoO_3 nanoparticles. Figure S1 (b) presents the FESEM micrographs of the synthesized samples which clearly display the 2D flake like morphology of the α-MoO_3 nanoparticles.

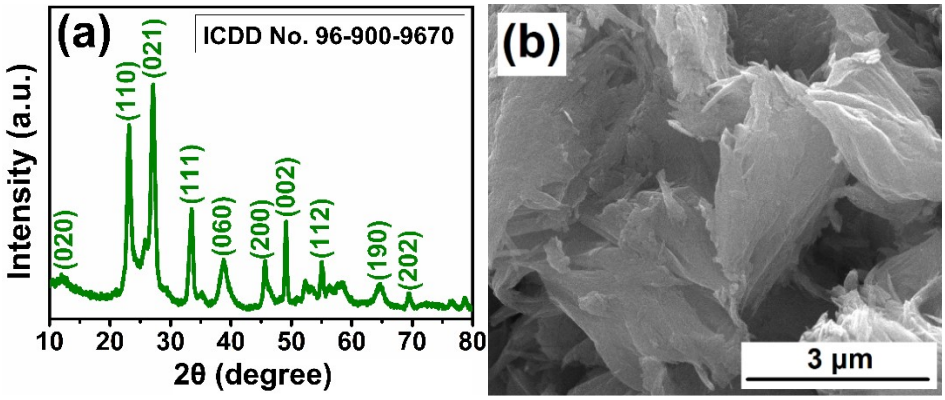

Figure S1: (a) XRD spectrum, and (b) FESEM micrographs of the 2D MoO_3 nanofiller.

S3 FESEM micrographs of the nanocomposites fabricated through the phase inversion method

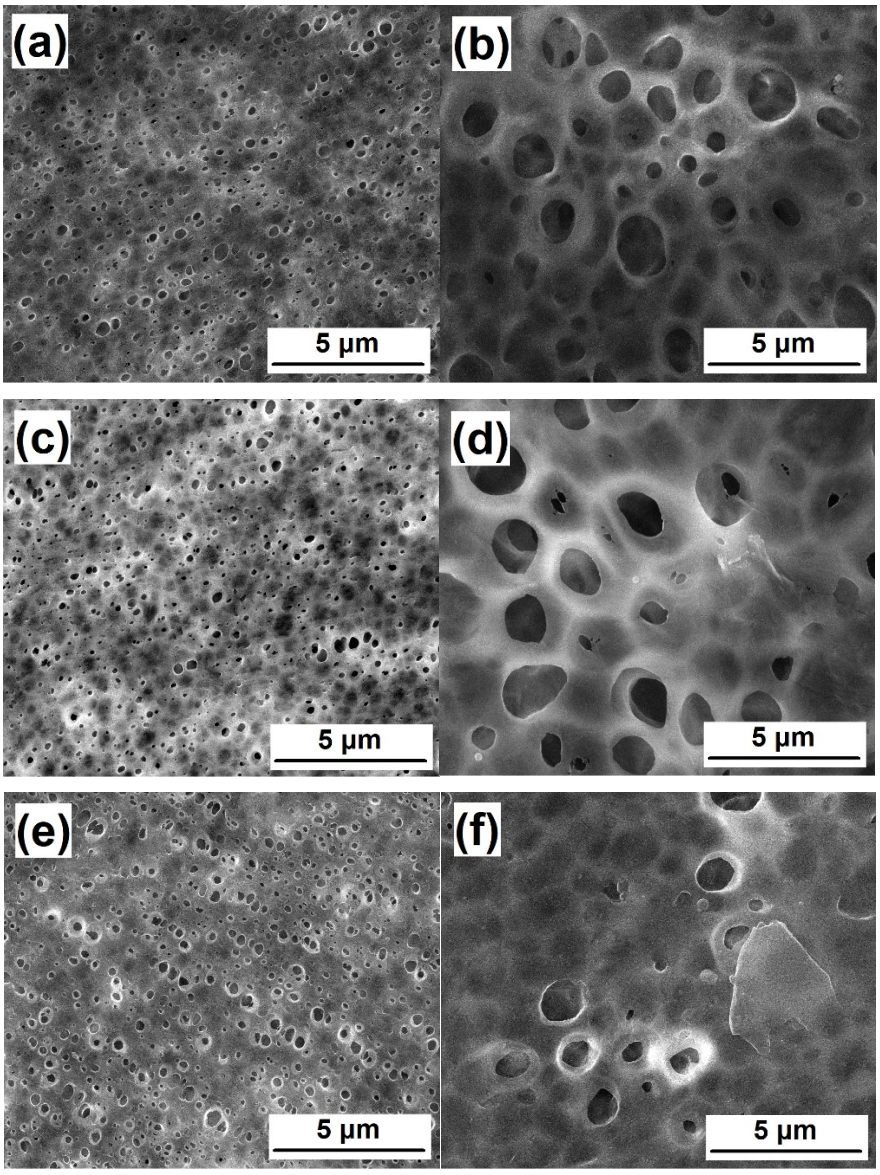

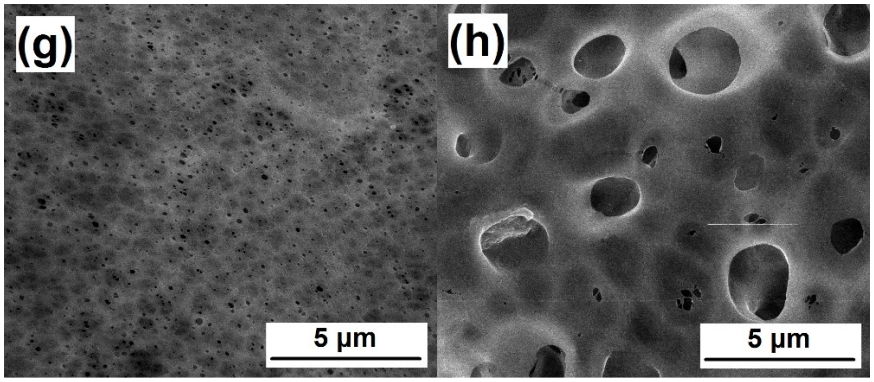

Figure S2: FESEM micrographs of the front and back faces of the nanocomposite films (a)-(b) MPI00, (c)-(d) MPI01, (e)-(f) MPI02, and (g)-(h) MPI04.

S4 Spinodal decomposition

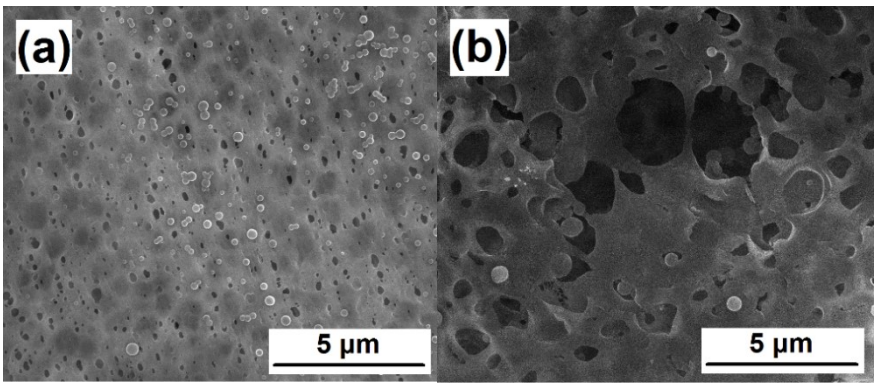

Figure S3: FESEM micrographs of the (a) front and (b) back faces of the MPI03 nanocomposite film showing the presence of spherical beads characteristic of spinodal decomposition.

S5 Porosity calculation of the fabricated nanocomposites

Quantitatively, the porosity of the nanocomposite films can be obtained using the n-butanol uptake method which gives the porosity (P) as[1]:

$$P(\%) = \frac{(M_{BuOH} - M_m)/\rho_{BuOH}}{(M_{BuOH} - M_m)\Big/\rho_{BuOH} + \dfrac{M_m}{\rho_p}} \times 100 \quad \ldots (1)$$

Here, M_m and M_{BuOH} are the masses of the dry film and n-butanol absorbed film, respectively, and ρ_p and ρ_{BuOH} are the densities of the polymer and n-butanol, respectively.

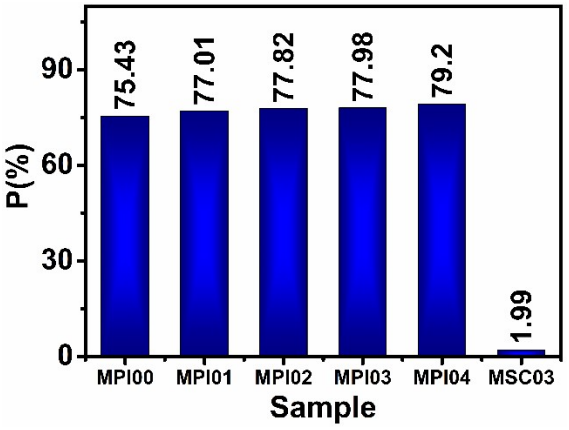

Figure S4: The comparison of the porosity of the various films obtained through phase inversion and solution casting technique.

S6 β-phase fraction [F(β)] calculation of the nanocomposites

The phase transformation of the porous nanocomposite films can be quantitatively analysed by calculating the β-phase fraction [F(β)] using the relation [2]:

$$F(\beta) = \frac{A_\beta}{\left(\frac{K_\beta}{K_\alpha}\right)A_\alpha + A_\beta} \quad \ldots (2)$$

Here, A_α and A_β are the obtained absorbance and K_α (6.1×10^4 cm^2 mol^{-1}) and K_β (7.7×10^4 cm^2 mol^{-1}) are the constant absorption coefficients at 764 cm^{-1} and 840 cm^{-1}, respectively.

S7 Comparative characterization of PI and SC film

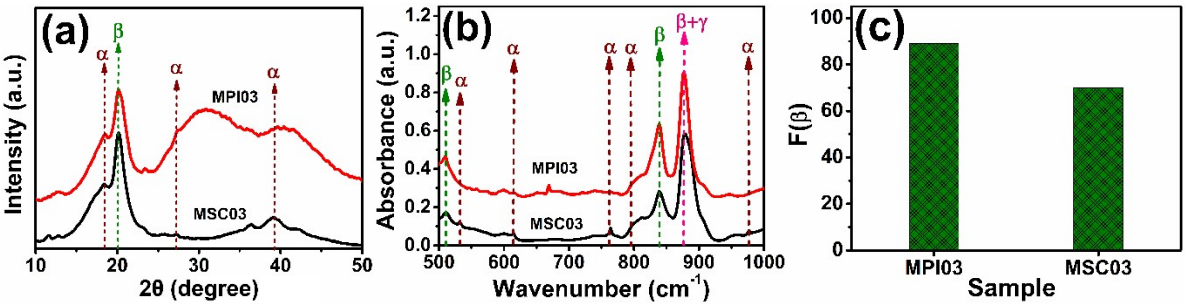

Figure S5: Comparison of the (a) XRD pattern, (b) FTIR spectra, and (c) the corresponding beta phase fraction of the nanocomposite film synthesized by the phase inversion method (MPI03) and solution casting method (MSC03), respectively.

S8. Triboelectric performance of MPI03 film based TENG

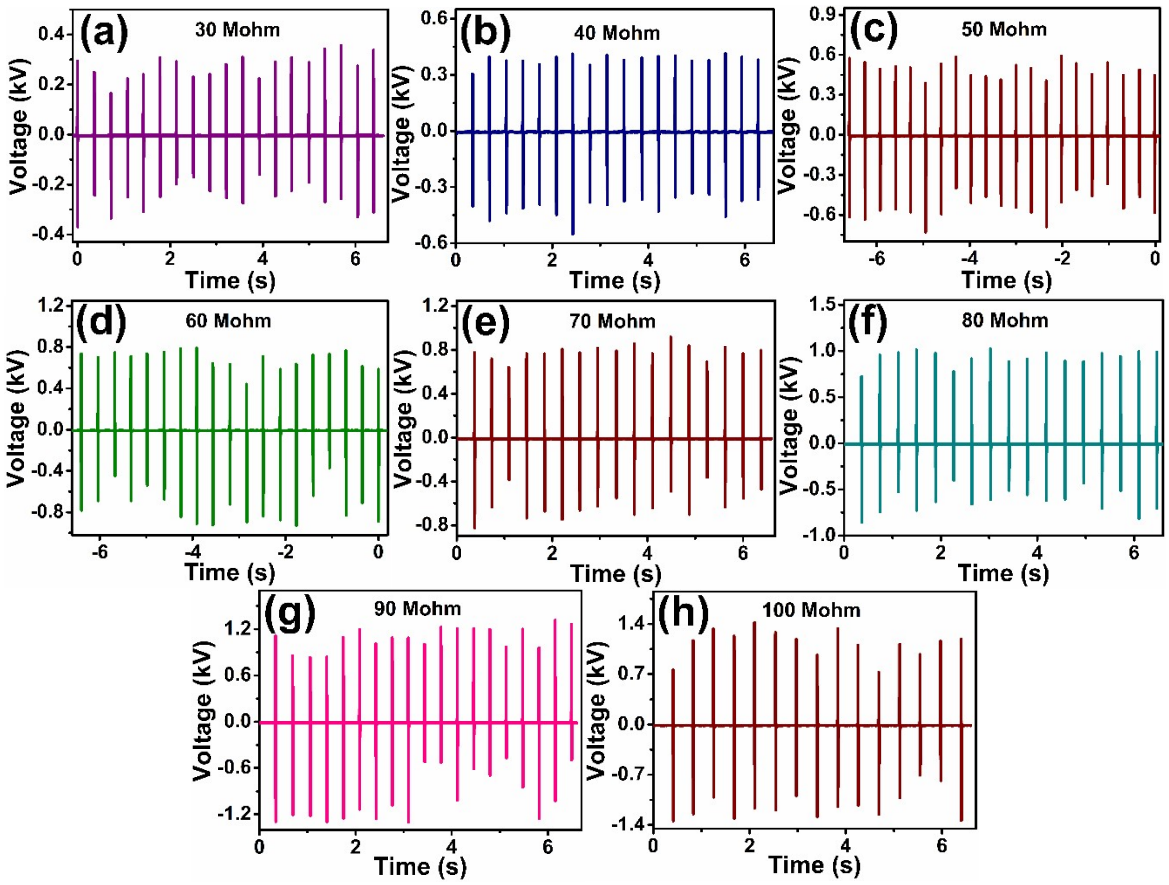

Figure S6: (a)-(h) Open-circuit output voltage from hand-tapped pressure imparting on the TENG fabricated using MPI03 composite film with load resistance varying from 30MΩ to 100 MΩ.

S9 Piezoelectric performance of MPI03 film based PENG

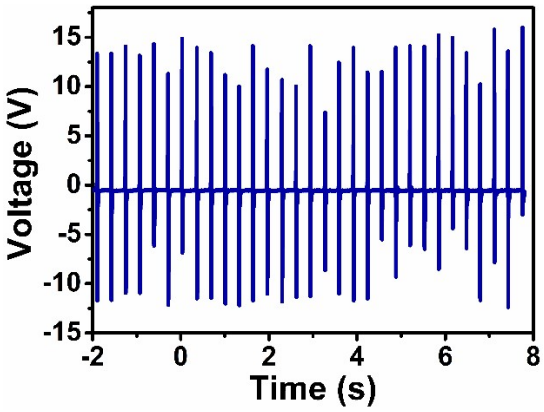

Figure S7: Energy harvesting performance of the piezoelectric nanogenerator fabricated using the MPI03 film

S10 Comparison of the tribolelectric performance of various 2D-nanofiller based TENGs

Energy harvesting system	Film synthesis method	Peak Voltage [V]	Power density $W.m^{-2}$	Ref.
Graphene/PVDF-HFP	Electrospinning	1024V at 10 N force	1.95	[3]
Graphene/PVDF	Thermal drawing	110V on hand tapping	53.57×10^{-3}	[4]
MoS_2/PVDF-HFP	Electrospinning	208 V at 25 N force	1.42	[5]
Mxene/PVDF	Sputtering	420V at 3 Hz frequency	619×10^{-3}	[6]
2D BN/PVDF	Electrospinning	500V at 50 N force	3.13	[7]
2D $MoTe_2$/PVDF	Electrospinning	319 V at 12 N force	2.9	[8]
Borophene/PVDF	Electrospinning	102.5 V on hand tapping	0.08	[9]
2D ZNO/$ZnSnO_3$-PVDF	Phase inversion	625 V at 80 N force	1.8	[10]
2D smectite clay/PVDF	Spin coating	104 V at 20 N force	1.45	[11]
2D α-MoO_3/PVDF-HFP	**Phase inversion**	**1100 V on hand tapping**	**8.08**	**This work**

Table S1: A comparison of the performance of the PI-TENG with other similar works reported in the literature.

S11 Short-circuit current measurement

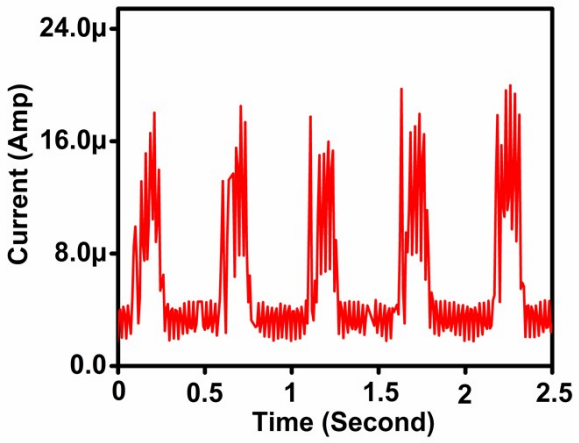

Figure S8: Short circuit current from hand-tapped pressure imparting on the TENG fabricated using MPI03 composite film.

S12 Capacitor charging performance of the TENGs

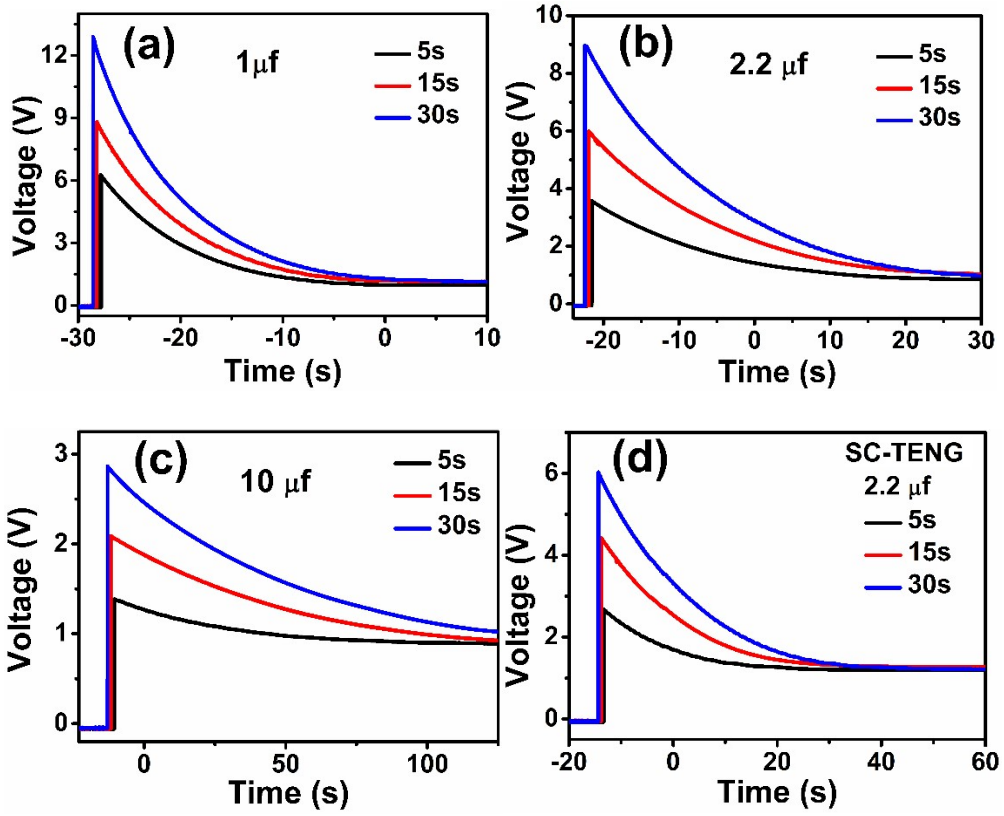

Figure S9: The discharging proces of (a) 1μF, (b) 2.2 μF, and (c) 10 μF capacitor as charged by hand tapping motion on the MPI03 TENG at different durations of 5s, 15s, and 30s. (d) The discharging process of a 2.2 μF capacitor charged by the hand-tapping motion on the MSC03 TENG at different durations of 5s, 15s, and 30s.

S13 FFT analysis of the output voltages obtained at different wrist bending positions

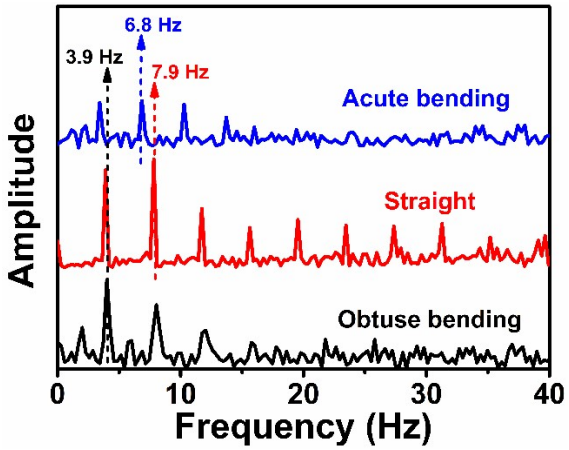

Figure S10: The frequency spectrum having distinct peak frequencies obtained from the FFT analysis of the output voltages of the TENG at different bending angles when attached to a human wrist.

References

1 J. Zhang, B. Sun, X. Huang, S. Chen and G. Wang, *Sci Rep*, 2014, 4, 1–7.

2 B. Dutta, E. Kar, N. Bose and S. Mukherjee, *RSC Adv*, 2015, 5, 105422–405434.

3 C. H. Lee, W. K. Huang, M. F. Lin, Y. H. Kuo, S. J. Liu and H. Ito, *RSC Adv*, 2024, 14, 38416–38425.

4 M. S. Bin Sadeque, M. Rahman, M. M. Hasan and M. Ordu, *Adv Electron Mater*, DOI:10.1002/aelm.202300643.

5 H. Zhao, J. H. Lin, H. T. Ren, H. kai Peng, C. W. Lou and T. T. Li, *Chemical Engineering Journal*, 2025, 505, 159107.

6 Y. Tao, H. Xiang, X. Cao and N. Wang, *ACS Appl Mater Interfaces*, 2024, 16, 3406–3415.

7 Z. Yang, X. Zhang and G. Xiang, *ACS Appl Nano Mater*, 2022, 5, 16906–16911.

8 D. Sarkar, N. Das, S. Sau, R. Basu and S. Das, *J Mater Chem C Mater*, 2023, 12, 984–1001.

9 N. K. Das, S. Chahal and S. Badhulika, *Mater Sci Semicond Process*, 2024, 180, 108555.

10 A. A. Narasimulu, P. Zhao, N. Soin, K. Prashanthi, P. Ding, J. Chen, S. Dong, L. Chen, E. Zhou, C. D. Montemagno and J. Luo, *Nano Energy*, 2017, 40, 471–480.

11 W. Li, F. Yan, Y. Xiang, W. Zhang, K. Loos and Y. Pei, *Nano Energy*, 2023, 112, 108487.